SAND2014-XXXR
LDRD PROJECT NUMBER: 158785
LDRD PROJECT TITLE:
Learning From Nature: Biomimetic Polarimetry for Imaging in Obscuring Environments
PROJECT TEAM MEMBERS:
John D. van der Laan, David A. Scrymgeour, Shanalyn A. Kemme

ABSTRACT: (250 WORDS)

We find for infrared wavelengths there are broad ranges of particle sizes and refractive indices that represent fog and rain where the use of circular polarization can persist to longer ranges than linear polarization. Using polarization tracking Monte Carlo simulations for varying particle size, wavelength, and refractive index systematically, we show that for specific scene parameters circular polarization outperforms linear polarization in maintaining the intended polarization state for large optical depths. This enhancement in circular polarization can be exploited to improve range and target detection in obscurant environments that are important in many critical sensing applications. Specifically, circular polarization persists better than linear for radiation fog in the short-wave infrared, for advection fog in the short-wave infrared and the long-wave infrared, and large particle sizes of Sahara dust around the 4 micron wavelength.

INTRODUCTION:

Polarized light propagation in scattering environments has been of recent interest where polarization sensing techniques increase range and contrast in these environments. Polarization offers an added variable to a sensing system that can be manipulated, to better discriminate a target from a scene and sense to greater depths in scattering environments. Previous research often has developed simulations and experiments utilizing polystyrene microspheres, milk, or tissue phantoms in water as the scattering environment of interest. Passive and active incoherent, polarizing systems in underwater environments use both linear and circular to reduce the effects of scattering. [1–3] More recently, Tyo analytically shows improved resolution from a narrower point spread function due to the difference between the amplitude-squared of the linearly polarized components compared to the sum of the amplitude-squared of the linearly polarized components. [4]

Silverman, et al. showed a factor of 2 – 3 increase in contrast using an active 544 nm polarization-modulated laser while imaging through 1 micron latex spheres in water. They investigated both linear and circular polarization showing better contrast with circular polarization. [5] Similarly, Dubreuil et al. investigated increased contrast with linear and circular polarization methods in varying concentrations of milky water solutions with polarization maintaining and depolarizing objects using a He-Ne laser for

illumination. [6] Sankaran, et al. looked at both circular and linear polarized light persistence through 1) three different sizes of polystyrene microspheres (0.107, 0.48, and 1.072 microns) in water, 2) a tissue phantom with polystyrene spheres ranging from 25 to 675 nm, and 3) several samples (porcine fat blood, tendon, heart, and artery tissue) at a wavelength of 632.8 nm. Circular polarization was shown to persist for larger particle sizes of microspheres but not for all tissue samples. [7-8] Through simulations and experiments Bartel et al. investigated the characteristics of 543 nm polarized light backscattered from polystyrene microsphere solutions with diameters of 204 nm and 2040 nm, specifically producing full backscattered Mueller matrices for the solutions. [9] Lewis, et al. published target contrast advantages of a factor of 4 for circular polarization-difference imaging versus linear polarization and a factor of 20 for circular polarization-difference imaging versus intensity imaging. They used 0.1 micron polystyrene spheres in water with a single active illumination wavelength of 632.8 nm. [10] Kartazayeva, et al. similarly investigated imaging techniques utilizing circular and linear polarization through large-diameter (10.143 microns) and small-diameter (0.202 microns) polystyrene particles with an active illumination of 632.8 nm, showing a factor of 3 increased contrast for circular polarization imaging versus linear polarization imaging. [11] Bicout, et al. showed through simulations and experiments that circular polarization persisted further than linear polarization for size parameters of 2.69, and 5.89 of latex spheres in water. [12] Ishimaru, et al. produced similar results for a size distribution of latex particles (~ 2 microns) in water with a single illuminating wavelength of 530 nm. [13]

Most of these previously published works are experimental measurements, utilizing a distinct, visible illuminating wavelength in a water environment. Three of these efforts include simulation. In contrast, our research identifies broad wavebands that demonstrate circular polarization's superiority in particle size and refractive index parameter sets that realistically model fog and dust in the atmosphere, through simulation. Recently, Miller, et al. utilized circular polarization difference imaging techniques to increase image contrast (by more than a factor of 10) in laboratory water vapor scenes; however, his work was also limited to a single visible illuminating wavelength. [14] Fade, et al. experimented in outdoor fog conditions imaging a polarized incandescent source but only utilized linear polarization for both illumination and detection. [15] These recent publications add to the previously published work in this area but are still limited in their incident illuminating wavelength. Our simulations remain unique in that they involve broad wavebands and identify circular polarization's role in realistic environments, through particle size and refractive index parameter ranges.

All sensing techniques using polarization in scattering environments rely on the polarization persistence of light, often called polarization memory. Techniques typically utilize the effect of a difference between the illuminating polarization that persists to the target and the polarization response of the scattering environment. [16] Circular polarization is of increasing interest due to its potentially superior persistence in scattering environments. The mechanism behind circular polarization's superior polarization persistence has been analytically explored by Xu and Alfano. They hypothesize that the two mechanisms that depolarize circularly polarized light, and therefore affect its persistence, are the randomization of the photons direction and the randomization of the helicity. They find that circular polarization persists superiorly for

large, soft particles and small, high index particles, which allow for increased uncoiling lengths. [17]

To date, no research has simulated or experimentally shown circular polarization's persistence benefits over a broad wavelength and sensing environment response. The majority of currently available experimental and simulation results, characterizing circular polarization, is limited to select wavelengths, typically in the visible spectrum, and utilize underwater scenes with varying concentrations of polystyrene microspheres, milk, or tissue phantoms as scattering objects. In this work we quantify a broad wavelength response at infrared wavelengths in multiple scattering environments where circular polarization sensing will outperform linear polarization.

Using Monte Carlo simulations, we model particle sizes and refractive indices representative of fog and dust at infrared wavelengths where circular polarization persists in the intended polarization at larger optical thicknesses than linear polarization. The increased persistence of circularly polarized light versus linear is shown for transmission and reflection through environments of fog and dust. Reflection results for these environments can also be found in our previously published conference paper. [18] The persistence of circular polarization in scattering environments can be exploited to improve sensing and imaging range in scattering environments, important to many critical applications.

This report is organized as follows: Experiment/Method section covers the background of polarization and the polarization Monte Carlo simulations, including validation of the simulation's performance against previously published work, the Results section explains the environments of interest and the parameters used for each set of simulations and presents the results for each of the environments of interest, the Discussion section explains in detail where circular polarization performs superiorly, the Anticipated Impact sections shows where and how this research is valuable for the national security mission at Sandia National Laboratories, and the Conclusion section sums up the report showing circular polarization persists better than linear polarization for certain scattering environments in all of the infrared regions, short-wave infrared (SWIR) 0.9-2.5 microns, mid-wave infrared (MWIR) 3-5 microns, and the long-wave infrared (LWIR) 8-12 microns.

DETAILED DESCRITPTION OF EXPERIMENT/METHOD:

Traditionally, when sensing in scattering environments the use of longer wavelengths is preferred due the decreased backscatter of the wavelengths through the environment of interest versus visible wavelengths. The longer wavelengths increase the number of particles that are considered in the Rayleigh scattering regime where scattering is isotropic. Also, the scattering cross-section of the particles is decreased with increased wavelength. [19] As a result, infrared wavelengths are considered superior to visible wavelengths in scattering environments of smaller particle sizes and smaller optical thicknesses. For highly scattering environments with large optical thicknesses all wavelengths are detrimentally affected. [20] In order to accurately sense targets in these challenging environments, all tools should be utilized. One such tool is the additional information available beyond intensity and wavelength of light, which is its polarization.

Polarization defines the movement of the electric field vector in space and time. The polarization of light is described by the Stokes parameters which are a part of the 4x1 Stokes vector,

$$\vec{S} = \begin{bmatrix} S_0 \\ S_1 \\ S_2 \\ S_3 \end{bmatrix} \propto \begin{bmatrix} I_H + I_V \\ I_H - I_V \\ I_{45} - I_{135} \\ I_R - I_L \end{bmatrix}, \tag{1}$$

where S_0 is the total intensity of the light, S_1 is the difference between linear horizontally polarized and linear vertically polarized flux, S_2 give the difference between the linear 45° polarized and linear 135° flux, and S_3 gives the difference between right and left circularly polarized flux. [21] A general Stokes vector is made up of a combination of a purely polarized portion and a completely unpolarized portion. The percentage of the total intensity that is purely polarized is defined as the Degree of Polarization (DoP).

$$DoP = \frac{\sqrt{{S_1}^2 + {S_2}^2 + {S_3}^2}}{S_0} \tag{2}$$

The DoP can vary between 0 (completely unpolarized light) to 1 (purely polarized light). Any Stokes vector with a DoP between 0 and 1 is partially polarized and can be separated into its purely polarized and unpolarized Stokes vectors shown in Equation 3.

$$\vec{S} = \vec{S}_{polarized} + \vec{S}_{unpolarized}$$

$$= \begin{bmatrix} \sqrt{{S_1}^2 + {S_2}^2 + {S_3}^2} \\ S_1 \\ S_2 \\ S_3 \end{bmatrix} + \begin{bmatrix} S_0 - \sqrt{{S_1}^2 + {S_2}^2 + {S_3}^2} \\ 0 \\ 0 \\ 0 \end{bmatrix} \tag{3}$$

In highly scattering environments, photons are multiply scattered and their polarization is mixed. Individual photons polarization states are randomized through the scattering process and the resulting transmitted and reflected polarization state is subsequently depolarized.

Our goal in this work is to investigate where circularly polarized light's persistence in highly scattering environments of real world interest is superior to linearly polarized light. To this end, we use a polarization tracking Monte Carlo program to investigate circularly polarized light's performance. [22] The Monte Carlo program tracks the polarization state of each photon in the simulation after every scattering event as they are propagated through a slab of scattering particles, Mie and/or Rayleigh sized. For each simulation run, one million photons of each polarization state were propagated into the slab of scattering medium. If the photons exit the front face of the slab they are considered transmitted photons, if the photons exits the back face of the slab they are

considered reflected or backscattered photons. For each simulation, a set of inputs are selected; these inputs are shown in Table 1.

Table 1: Monte Carlo inputs and definitions.

Input	Symbol	(units)
Particle Diameter	D	(μm)
Wavelength (vacuum)	λ_0	(μm)
Particle Refractive Index	$n_p - i\,k_p$	
External Medium Refractive Index	$n_m - i\,k_m$	
Relative Refractive Index	$m = \frac{n_p - i\,k_p}{n_m - i\,k_m}$	
Particle Density	ρ	(particles/mm^3)
Slab Length	L	(cm)

From these inputs, the Monte Carlo utilizes Mie Scattering Theory for homogenous spherical particles to determine the single scattering properties of the scattering objects. [19] These inputs also give the overall optical thickness of the slab of scattering particles for each simulation configuration. The optical thickness, τ, is defined by the previously stated terms and the scattering cross-section, C_{sca}, determined from Mie Scattering Theory.

$$\tau = \rho\, C_{sca}\, L \tag{4}$$

We utilized published numbers in order to verify our Monte Carlo simulation's output. Ishimaru, et. al. performed simulations looking at circular and linear polarizations transmitted DoP versus optical thickness for a specific scattering environment. [13] The environment of interest was 1.05 micron diameter latex spheres in water with an illumination wavelength of 0.53 microns. We performed similar simulations with our Monte Carlo program and we see confirmation with Ishimaru's results. Fig. 1 shows Ishimaru's results as a solid and dotted line with our simulation results shown as circles and squares.

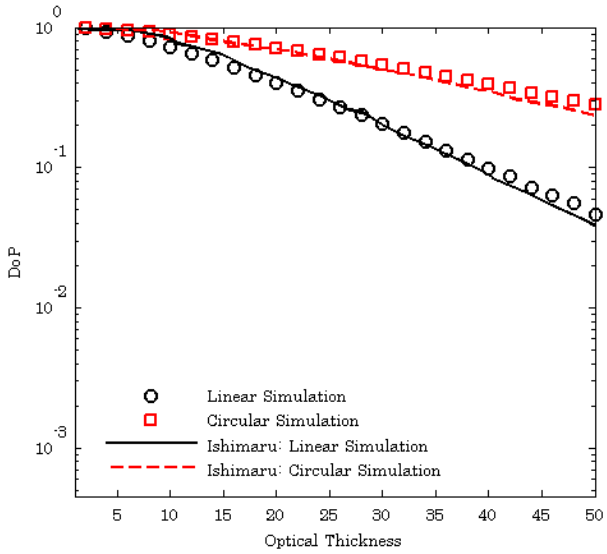

Fig. 1. Ishimaru's simulated transmission results (solid black and dashed red lines) [13] versus our confirming simulated transmission results (black circles and red squares) for 1.05 micron diameter latex spherical particles in water with an illumination wavelength of 0.53 microns

Before moving onto the environments of interest and our results we must define one more useful quantity. Throughout our analysis we are specifically interested in the performance difference between circular and linear incident polarization states on the slab of scattering medium. To clearly determine where circularly polarized light outperforms linearly polarized light a difference quantity is defined. The quantity, DoP_{diff}, is defined as the difference between the resulting transmitted or reflected DoP when circularly polarized light is incident versus when linearly polarized light is incident. The definition is defined in Equation 5.

$$DoP_{diff} = DoP_{circular} - DoP_{linear} \tag{5}$$

When circularly polarized light transmits or reflects with a higher DoP than linearly polarized light this quantity is positive. This quantity is negative when linearly polarized light transmits or reflects with a larger DoP. For our analysis it is of particular interest when the DoP_{diff} is positive and circularly polarized light maintains its DoP better than linearly polarized light, persisting superiorly.

RESULTS:

For each environment, one million photons of both circular and linear polarizations were launched into a slab of the specific particles. The resulting transmitted or reflected DoP was calculated and the DoP_{diff} was determined. The following figures show the DoP_{diff} versus wavelength for each environment. In order to better delineate where circularly polarized light outperforms linearly polarized light a line is plotted for a $DoP_{diff} = 0$.

Environments

Four realistic scattering environments were simulated: two types of fog (radiation and advection) and two types of Sahara dust (small and large). Three particle diameters were chosen from the particle size range for each environment. The particle sizes were chosen to coincide with small, large, and mean diameter sizes from the environments particle diameter distribution. All simulations were run with mono-disperse particle diameters at optical thicknesses of 5 in order to clearly see variations in performance due to particle size variation.

The first two environments simulated were two types of fog. The table below shows the size parameter for different particle sizes at each wavelength. The size parameter is an important value used in the Mie Theory calculations. The size parameter is defined as,

$$x = \frac{2\,\pi\,r}{\lambda},$$

where r is the particle radius. The particle sizes simulated were chosen to cover a large, small, and mean value of the typical log-normal particle size distribution for each fog. The table shows highlights what particle sizes are typical for each type of fog and where there is overlap. Light blue indicates sizes for radiation fog, dark blue indicates sizes for advection fog, and the medium blue indicates where both types of fog have particles in that size.

Table 2: Size parameter values for fog at infrared wavelengths. Light blue indicates size range for radiation fog, dark blue indicates sizes for advection fog, and the medium blue indicates where both fog types overlap.

		Wavelength (microns)																	
		SWIR			MWIR					LWIR									
		1	1.5	2	3	3.5	4	4.5	5	8	8.5	9	9.5	10	10.5	11	11.5	12	
Particle Diameter (microns)	1	3.1	2.1	1.6	1.0	0.9	0.8	0.7	0.6	0.4	0.4	0.3	0.3	0.3	0.3	0.3	0.3	0.3	
	2	6.3	4.2	3.1	2.1	1.8	1.6	1.4	1.3	0.8	0.7	0.7	0.7	0.6	0.6	0.6	0.5	0.5	
	3	9.4	6.3	4.7	3.1	2.7	2.4	2.1	1.9	1.2	1.1	1.0	1.0	0.9	0.9	0.9	0.8	0.8	
	4	12.6	8.4	6.3	4.2	3.6	3.1	2.8	2.5	1.6	1.5	1.4	1.3	1.3	1.2	1.1	1.1	1.0	
	5	15.7	10.5	7.9	5.2	4.5	3.9	3.5	3.1	2.0	1.8	1.7	1.7	1.6	1.5	1.4	1.4	1.3	
	6	18.8	12.6	9.4	6.3	5.4	4.7	4.2	3.8	2.4	2.2	2.1	2.0	1.9	1.8	1.7	1.6	1.6	
	7	22.0	14.7	11.0	7.3	6.3	5.5	4.9	4.4	2.7	2.6	2.4	2.3	2.2	2.1	2.0	1.9	1.8	
	8	25.1	16.8	12.6	8.4	7.2	6.3	5.6	5.0	3.1	3.0	2.8	2.6	2.5	2.4	2.3	2.2	2.1	
	9	28.3	18.8	14.1	9.4	8.1	7.1	6.3	5.7	3.5	3.3	3.1	3.0	2.8	2.7	2.6	2.5	2.4	
	10	31.4	20.9	15.7	10.5	9.0	7.9	7.0	6.3	3.9	3.7	3.5	3.3	3.1	3.0	2.9	2.7	2.6	
	11	34.6	23.0	17.3	11.5	9.9	8.6	7.7	6.9	4.3	4.1	3.8	3.6	3.5	3.3	3.1	3.0	2.9	
	12	37.7	25.1	18.8	12.6	10.8	9.4	8.4	7.5	4.7	4.4	4.2	4.0	3.8	3.6	3.4	3.3	3.1	
	13	40.8	27.2	20.4	13.6	11.7	10.2	9.1	8.2	5.1	4.8	4.5	4.3	4.1	3.9	3.7	3.6	3.4	
	14	44.0	29.3	22.0	14.7	12.6	11.0	9.8	8.8	5.5	5.2	4.9	4.6	4.4	4.2	4.0	3.8	3.7	
	15	47.1	31.4	23.6	15.7	13.5	11.8	10.5	9.4	5.9	5.5	5.2	5.0	4.7	4.5	4.3	4.1	3.9	
	16	50.3	33.5	25.1	16.8	14.4	12.6	11.2	10.1	6.3	5.9	5.6	5.3	5.0	4.8	4.6	4.4	4.2	

17	53.4	35.6	26.7	17.8	15.3	13.4	11.9	10.7	6.7	6.3	5.9	5.6	5.3	5.1	4.9	4.6	4.5
18	56.5	37.7	28.3	18.8	16.2	14.1	12.6	11.3	7.1	6.7	6.3	6.0	5.7	5.4	5.1	4.9	4.7
19	59.7	39.8	29.8	19.9	17.1	14.9	13.3	11.9	7.5	7.0	6.6	6.3	6.0	5.7	5.4	5.2	5.0
20	62.8	41.9	31.4	20.9	18.0	15.7	14.0	12.6	7.9	7.4	7.0	6.6	6.3	6.0	5.7	5.5	5.2
21	66.0	44.0	33.0	22.0	18.8	16.5	14.7	13.2	8.2	7.8	7.3	6.9	6.6	6.3	6.0	5.7	5.5
22	69.1	46.1	34.6	23.0	19.7	17.3	15.4	13.8	8.6	8.1	7.7	7.3	6.9	6.6	6.3	6.0	5.8
23	72.3	48.2	36.1	24.1	20.6	18.1	16.1	14.5	9.0	8.5	8.0	7.6	7.2	6.9	6.6	6.3	6.0
24	75.4	50.3	37.7	25.1	21.5	18.8	16.8	15.1	9.4	8.9	8.4	7.9	7.5	7.2	6.9	6.6	6.3
25	78.5	52.4	39.3	26.2	22.4	19.6	17.5	15.7	9.8	9.2	8.7	8.3	7.9	7.5	7.1	6.8	6.5
26	81.7	54.5	40.8	27.2	23.3	20.4	18.2	16.3	10.2	9.6	9.1	8.6	8.2	7.8	7.4	7.1	6.8
27	84.8	56.5	42.4	28.3	24.2	21.2	18.8	17.0	10.6	10.0	9.4	8.9	8.5	8.1	7.7	7.4	7.1
28	88.0	58.6	44.0	29.3	25.1	22.0	19.5	17.6	11.0	10.3	9.8	9.3	8.8	8.4	8.0	7.6	7.3
29	91.1	60.7	45.6	30.4	26.0	22.8	20.2	18.2	11.4	10.7	10.1	9.6	9.1	8.7	8.3	7.9	7.6
30	94.2	62.8	47.1	31.4	26.9	23.6	20.9	18.8	11.8	11.1	10.5	9.9	9.4	9.0	8.6	8.2	7.9
31	97.4	64.9	48.7	32.5	27.8	24.3	21.6	19.5	12.2	11.5	10.8	10.3	9.7	9.3	8.9	8.5	8.1
32	100.5	67.0	50.3	33.5	28.7	25.1	22.3	20.1	12.6	11.8	11.2	10.6	10.1	9.6	9.1	8.7	8.4
33	103.7	69.1	51.8	34.6	29.6	25.9	23.0	20.7	13.0	12.2	11.5	10.9	10.4	9.9	9.4	9.0	8.6
34	106.8	71.2	53.4	35.6	30.5	26.7	23.7	21.4	13.4	12.6	11.9	11.2	10.7	10.2	9.7	9.3	8.9
35	110.0	73.3	55.0	36.7	31.4	27.5	24.4	22.0	13.7	12.9	12.2	11.6	11.0	10.5	10.0	9.6	9.2
36	113.1	75.4	56.5	37.7	32.3	28.3	25.1	22.6	14.1	13.3	12.6	11.9	11.3	10.8	10.3	9.8	9.4
37	116.2	77.5	58.1	38.7	33.2	29.1	25.8	23.2	14.5	13.7	12.9	12.2	11.6	11.1	10.6	10.1	9.7
38	119.4	79.6	59.7	39.8	34.1	29.8	26.5	23.9	14.9	14.0	13.3	12.6	11.9	11.4	10.9	10.4	9.9
39	122.5	81.7	61.3	40.8	35.0	30.6	27.2	24.5	15.3	14.4	13.6	12.9	12.3	11.7	11.1	10.7	10.2
40	125.7	83.8	62.8	41.9	35.9	31.4	27.9	25.1	15.7	14.8	14.0	13.2	12.6	12.0	11.4	10.9	10.5

1. Radiation Fog

Radiation fog is the first environment simulated. Radiation fog is typically found near the ground, sometimes called ground fog, and arises when the earth cools thermally after the sun sets. The typical model for radiation fog consist of water particles with diameters smaller than 10 microns. [23–25] In order to simulate the range of particle sizes, three particle diameters were chosen: 1, 4, and 10 micron diameters.

The following two figures show results for radiation fog from the SWIR wavelength regime for reflection and transmission.

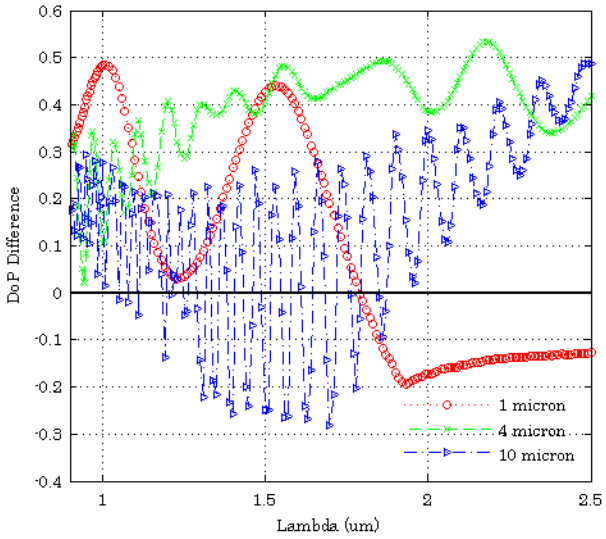

Fig. 2: Reflection DoP_{diff} results for radiation fog for SWIR wavelengths. 1 micron particle size results shown in red (circles), 4 micron particle size results shown in green (x's), and 10 micron particle size results shown in blue (triangles). A black line for $DoP_{diff} = 0$ delineates where linear polarization performs better (negative values) and where circular polarization performs better (positive values).

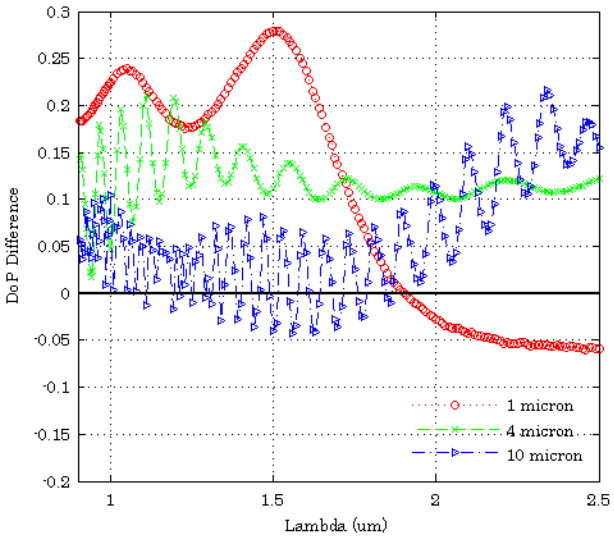

Fig. 3: Transmission DoP_{diff} results for radiation fog for SWIR wavelengths. 1 micron particle size results shown in red (circles), 4 micron particle size results shown in green (x's), and 10 micron particle size results shown in blue (triangles). A black line for $DoP_{diff} = 0$ delineates where linear polarization performs better (negative values) and where circular polarization performs better (positive values).

The radiation fog results for the MWIR through the LWIR for reflection and transmission are shown in the following two figures.

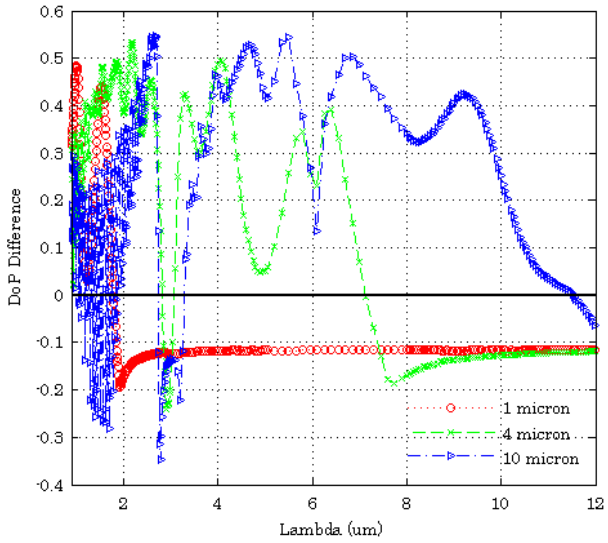

Fig. 4: Reflection DoP_{diff} results for radiation fog for SWIR through LWIR wavelengths. 1 micron particle size results shown in red (circles), 4 micron particle size results shown in green (x's), and 10 micron particle size results shown in blue (triangles). A black line for $DoP_{diff} = 0$ delineates where linear polarization performs better (negative values) and where circular polarization performs better (positive values).

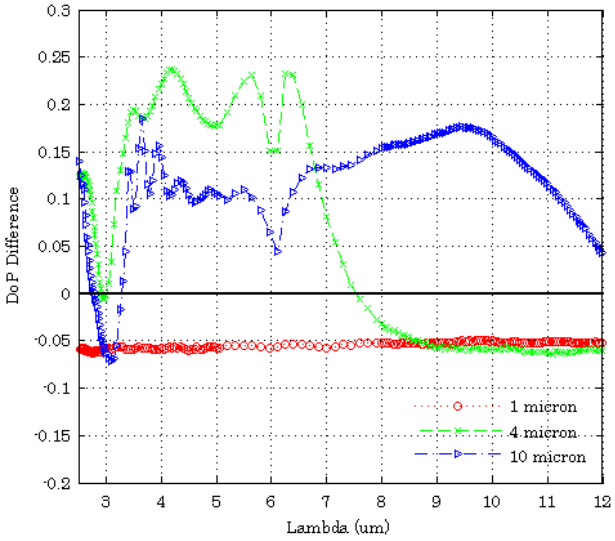

Fig. 5: Transmission DoP_{diff} results for radiation fog for MWIR through LWIR wavelengths. 1 micron particle size results shown in red (circles), 4 micron particle size results shown in green (x's), and 10 micron particle size results shown in blue (triangles). A black line for $DoP_{diff} = 0$ delineates where linear polarization performs better (negative values) and where circular polarization performs better (positive values).

2. Advection Fog

Advection fog was the second fog simulated. Advection fog is typically found near coastlines and marine environments. When wind moves water-dense air over colder surfaces, such as warm air traveling over cool waters, the air is cooled and advection fog is produced. Typical models of advection fog consist of larger particle sizes compared to radiation fog. [25] For our purposes we model advection fog as three particles diameters,

10, 20, and 40 microns. For both radiation and advection fog the index values for water were taken from data measured and collected by Segelstein. [26]

Results for the advection fog simulations are shown in the following three figures. The reflection results are shown first for all wavelengths, SWIR to LWIR. The latter two figures show the transmission results for advection fog. The first of the transmission figures shows the SWIR wavelength results, while the last figure shows the transmission results for the MWIR to LWIR wavelengths.

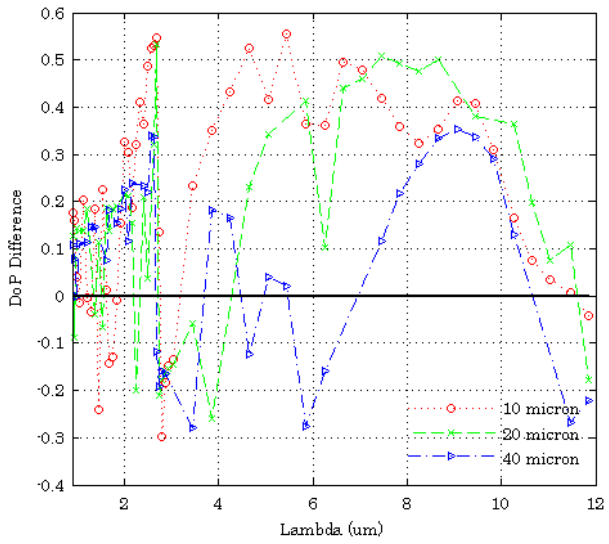

Fig. 6: Reflection DoP_{diff} results for advection fog for SWIR through LWIR wavelengths. 10 micron particle size results shown in red (circles), 20 micron particle size results shown in green (x's), and 40 micron particle size results shown in blue (triangles). A black line for $DoP_{diff} = 0$ delineates where linear polarization performs better (negative values) and where circular polarization performs better (positive values).

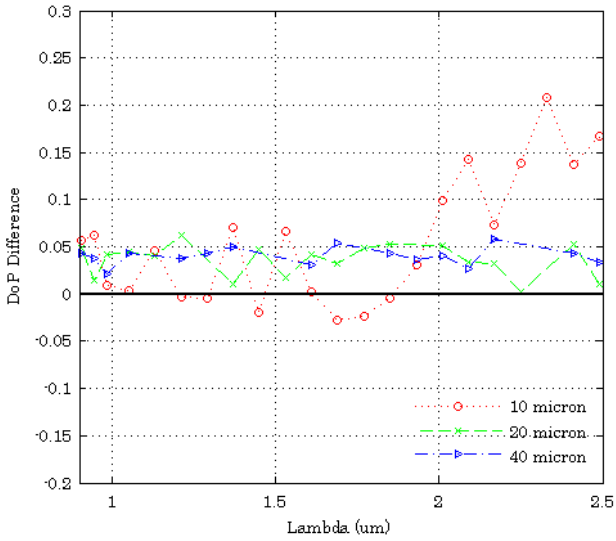

Fig. 7: Transmission DoP_{diff} results for advection fog for SWIR wavelengths. 10 micron particle size results shown in red (circles), 20 micron particle size results shown in green (x's), and 40 micron particle size results shown in blue

(triangles). A black line for $DoP_{diff} = 0$ delineates where linear polarization performs better (negative values) and where circular polarization performs better (positive values).

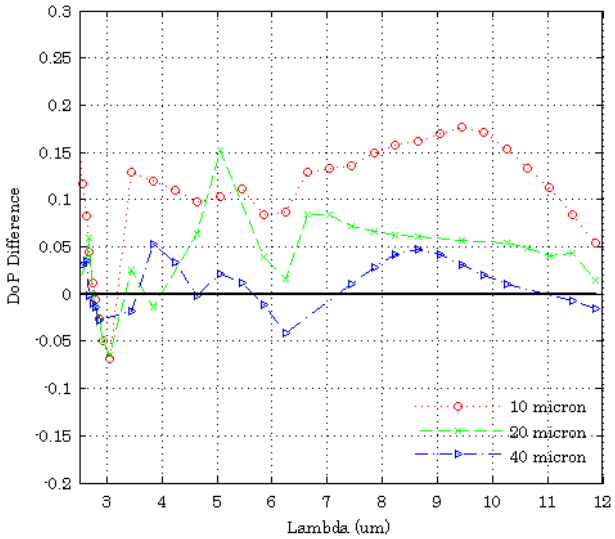

Fig. 8: Transmission DoP_{diff} results for advection fog for MWIR through LWIR wavelengths. 10 micron particle size results shown in red (circles), 20 micron particle size results shown in green (x's), and 40 micron particle size results shown in blue (triangles). A black line for $DoP_{diff} = 0$ delineates where linear polarization performs better (negative values) and where circular polarization performs better (positive values).

3. Small Particle Sahara Dust

The final two environments simulated were Sahara dust. The two different models illustrate small and large particles. The small particle Sahara dust sizes characterize dust that is typically suspended in various altitudes in the atmosphere. These small particle sizes are easily sent airborne and remain in the atmosphere for large distances. The diameters used for the small particle size model were 0.1, 1.5, and 6 microns. [27,28]

As there is no index data available from Volz, et al. for SWIR wavelengths, the results for Sahara dust were generated for the MWIR and LWIR regions only, using the available index data. [29] The reflection and transmission results for the small particle Sahara Dust simulations are shown in the following figures.

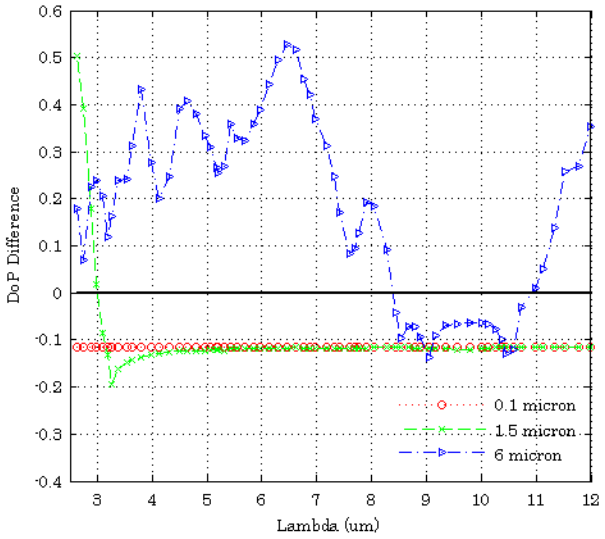

Fig. 9: Reflection DoP_{diff} for small particle diameters of Sahara Dust for MWIR through LWIR wavelengths. 0.1 micron particle size results shown in red (circles), 1.5 micron particle size results shown in green (x's), and 6 micron particle size results shown in blue (triangles). A black line for $DoP_{diff} = 0$ delineates where linear polarization performs better (negative values) and where circular polarization performs better (positive values).

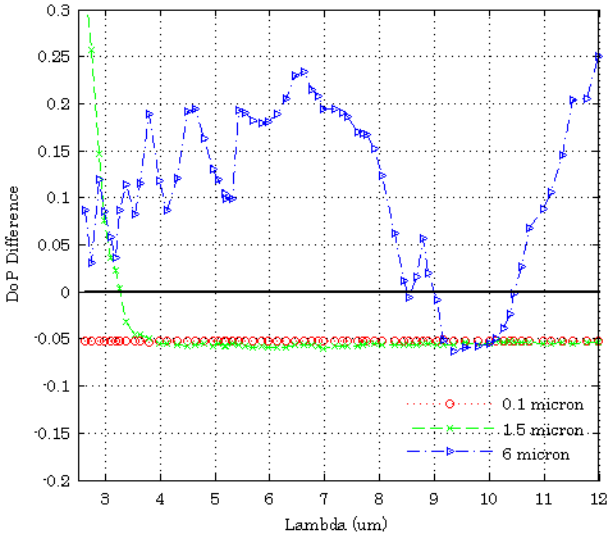

Fig. 10: Transmission DoP_{diff} for small particle diameters of Sahara Dust for MWIR through LWIR wavelengths. . 0.1 micron particle size results shown in red (circles), 1.5 micron particle size results shown in green (x's), and 6 micron particle size results shown in blue (triangles). A black line for DoP = 0 delineates where linear polarization performs better (negative values) and where circular polarization performs better (positive values).

4. Large Particle Sahara Dust

The large particle Sahara dust sizes characterize dust found nearer to earth's surface. [27,28] For the large particle size model, particle diameters of 10, 20, and 30 microns were used. Both the small and large particle models used Sahara dust and sand index information taken from Volz et. al. [29] The simulation results for Sahara dust all

involve simulations of homogeneous spherical particles. The authors are aware of the fact that typical dust particles can be highly non-spherical. Mie Theory is still used for many purposes with dust measurements and thus these results seek to open areas of further study and experimentation where circular polarization can be of benefit.

The results for the large particle Sahara dust model for the MWIR through the LWIR for reflection and transmission are shown in the following figures.

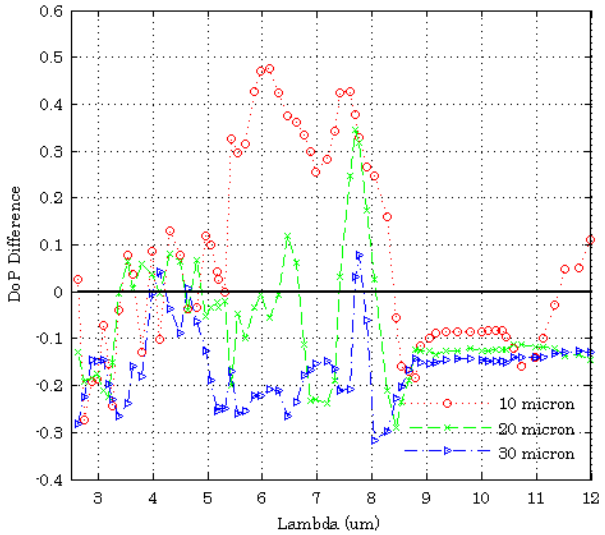

Fig. 11: Reflection DoP_{diff} for large particle diameters of Sahara Dust for MWIR through LWIR wavelengths. 10 micron particle size results shown in red (circles), 20 micron particle size results shown in green (x's), and 30 micron particle size results shown in blue (triangles). A black line for $DoP_{diff} = 0$ delineates where linear polarization performs better (negative values) and where circular polarization performs better (positive values).

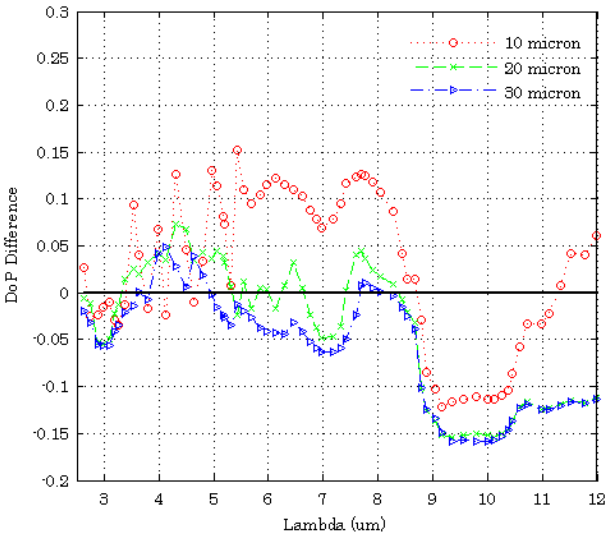

Fig. 12: Transmission DoP_{diff} for large particle diameters of Sahara Dust for MWIR through LWIR wavelengths. 10 micron particle size results shown in red (circles), 20 micron particle size results shown in green (x's), and 30 micron particle size results shown in blue (triangles). A black line for $DoP_{diff} = 0$ delineates where linear polarization performs better (negative values) and where circular polarization performs better (positive values).

DISCUSSION:

The following discussion focuses on the transmission results from the previous section. The overall results for reflection and transmission follow similar trends. In general, the difference between circular and linear polarization is larger for the reflection results. This is most likely due to the fact that the reflected light has a lower power and small variations can lead to large differences in the polarization. The transmission results have smaller DoP_{diff} values but there are typically fewer large oscillations due to the increased signal in transmission versus reflection. For this reason the transmission results will be the focus of this report's discussion.

Radiation Fog

The radiation fog results are shown in Fig. 2 and Fig. 3. Fig. 3 shows circularly polarized light outperforms linearly polarized light for all three particle sizes for SWIR wavelengths. Circular polarization persists superiorly for the 1 micron particle through a wavelength of 1.9 microns. The results for the 4 micron particle show some oscillation in the smaller wavelengths, but throughout the entire SWIR region circular polarization outperforms linear polarization. The 10 micron particle results show a preference for circular polarization throughout the SWIR region but this particle size shows a large amount of oscillatory behavior. At roughly a wavelength of 1.9 microns circular polarization clearly begins to persist superiorly for the 10 micron particle.

The radiation fog results for the MWIR through the LWIR are shown in Fig. 5. For both the MWIR and LWIR wavelengths, the small 1 micron particle shows preference for linearly polarized light. The two larger particle sizes show circular polarization persisting superiorly in the MWIR. The 4 micron particle has a larger DoP_{diff}, but circular polarization is clearly beneficial in this region. For the LWIR region, only the largest 10 micron particle size shows a persistence benefit for circularly polarized light. Linear polarization is preferred for both the 1 and 4 micron particles in the LWIR.

The simulation results show clear wavebands where circular polarization persists longer than linear polarization for radiation fog. The 1 micron particle shows circular polarization persists superiorly in the SWIR up to a wavelength of 1.9 microns. Circular polarization is superior for the 4 micron particle in the SWIR and MWIR regions. The 10 micron particle has a broad waveband where circular polarization persists better than linear. There are some oscillations in the lower end of the SWIR region but throughout the SWIR, MWIR, and the LWIR circular polarization is preferred and superior for the 10 micron particle.

Advection Fog

Results for the advection fog simulations are shown in Fig. 6, Fig. 7, and Fig. 8. Fewer data points were generated for each particle diameter for the advection results due to increased computation time for the larger particle sizes. For comparison, the 10 micron results for advection fog are the exact same as those for radiation fog, since the index and size is the same. The additional points available in the radiation results are omitted for congruency with the other sets of data in order to maintain the same number

of data points and to clarify the plots. The spectral resolution on the advection fog plots are thus lower than the radiation fog plots but the general patterns can still be observed.

The SWIR results are shown in Fig. 7. Similar to the radiation fog results, the 10 micron particle shows oscillations in the lower end of SWIR region but is generally positive for circular polarization. The 20 and 40 micron particles show a preference for circular polarization throughout the SWIR region. Due to the lower sample size and spectral resolution it is difficult to determine with certainty whether the larger particles maintain their circular polarization persistence benefit uniformly or if the oscillations are merely sampled out.

The MWIR and LWIR advection results are shown in Fig. 8. Once again the 10 micron clearly shows superior persistence for circular polarization throughout the MWIR and LWIR regions. There is some oscillatory behavior in the 3-4 micron wavelength range but after 4 microns the 20 micron particle shows a preference for circular polarization through to the end of the LWIR. The 40 micron particle is more limited in wavelengths showing beneficial persistence for circular polarization. There are multiple wavebands in the MWIR. Generally, circular is preferred from 3.5-5 microns, with a dip at 4.7 microns where circular and linear are equal in persistence. Circular polarization has increased persistence for the 40 micron particle through almost all of the LWIR, 7-11 microns.

Advection fog shows multiple clear wavebands where circular polarization persists longer than linear polarization. There are some oscillations in the SWIR region but generally all particle sizes show a preference for circular polarization. The MWIR region is mixed. Circular polarization is preferred for the 10 micron particle through the entire region, the 20 micron particle is positive after a wavelength of 4 microns, and the 40 micron particle oscillates but generally is positive for wavelengths greater than 3.5 microns in the MWIR. Throughout the LWIR regime all particle sizes show superior circular polarization persistence. All the particles show positive DoP_{diff} from 7-11 microns. The 40 micron particle is the only particle that shows any preference for linear polarization in the LWIR and it is only for wavelengths of 11-12 microns. In general, we can expect circular polarization to persist longer than linear polarization for the LWIR region from 7 to 11 microns with advection fog scattering particles with diameters spanning 10 and 40 microns.

Small Particle Sahara Dust

Fig. 9 and Fig. 10 show the results for the small particle Sahara dust model. Linear polarization dominates for the very small particle sizes of 0.1 and 1.5 microns. The 1.5 micron particles show possible promise at lower wavelengths. Circular polarization persists much better for the 1.5 micron particle from 2.5-3.25 microns. This performance may be positive in the SWIR region as well but is left for future investigation. For the larger 6 micron diameter particles, circular polarization persists better than linear throughout the MWIR region as well as the low and high end of the LWIR region. Between a wavelength of 9 and 10.5 microns the 6 micron particles show a persistence benefit for linear polarization.

Overall, only the 6 micron Sahara dust particles show broad wavebands where circular polarization persists longer than linear polarization, all of the MWIR region, up

to 9 microns, and 10.5 to 12 microns. The only other waveband for the particles is 2.5 to 3.25 microns for the 1.5 micron particle. Linear polarization persists longer for the smallest 0.1 micron particle. The large gap in particle sizes from 1.5 to 6 microns may offer additional particle sizes where the performance is closer to that of 6 micron diameter particles.

Large Particle Sahara Dust

The results for the large particle Sahara dust model for the MWIR through the LWIR are shown in Fig. 11 and Fig. 12. The 10 micron particle oscillates in the MWIR region but shows some preference for circular polarization from 3.5 to 5 microns. Circular polarization again persists superiorly in the low and high ends of the LWIR region. Specifically, circular polarization is preferred up to wavelengths of 8.75 microns and from 11.25 to 12 microns. The 20 micron particle has a small waveband where circular polarization superiorly persists. The waveband is from a wavelength of 3.25 to 5.5 microns. The 20 micron particle also has a positive DoP_{diff} value from 7.5 to 8.5 microns but generally linear polarization persists better in the LWIR for this particle size. The results for the 30 micron particle are nearly identical to the 20 micron particle results. The wavebands are slightly smaller and the overall performance is smaller than with the 20 micron particle.

For large particle Sahara dust environments circular polarization has limited wavelengths where it persists superiorly than linear polarization. All three particle show some positive performance near wavelengths of 3.5 to 5 microns. There is also a small waveband near a wavelength of 8 microns where all three particle sizes have positive performance.

ANTICIPATED IMPACT:

We have shown in this work that utilizing the polarization state of light can improve signal persistence, increasing range and thus improving target detection in scattering environments of fog and dust. Polarization optics can be readily added to current, traditional optical sensing systems in operation. Both active and passive configurations are possible, with benefits for each in certain situations. These systems can be used both in daytime and nighttime conditions. This research allows us to intelligently select wavebands for specific adverse imaging environments. Our work produces valuable insights into increased use of circular polarization in critical scattering environments of interest.

Sensing an object or target in a highly scattering environment is a challenge for many national security related situations. There is a multitude of environments in nature that deteriorate human and machine vision capabilities. The following section will highlight a few examples of these environments and where the results of this research may provide valuable techniques that can be utilized to detect targets at larger ranges.

Underwater imaging is an example of a scattering environment where imaging and target detection is a challenge. Typical water environments are filled with various scattering particles that degrade images and scatter and absorb light, in addition to the absorption of most wavelengths underwater. One new worthy example of this was during

the Deepwater Horizon oil spill, where robotic vehicles vision systems were restricted to visible wavelengths and intensity imaging. Circular polarization imaging techniques could be used to increase detection range in underwater environments for critical detection and imaging applications. Increasing the detection range in underwater environments is a valuable performance benefit. When a target or foreign object is present in an underwater scene determining is important and time-sensitive – increasing the detection range and contrast increases the time and distance available for decision making.

Environments which are obscured by fog are challenging to image and sense through much like underwater. Fog acts as a scattering particle in the atmosphere and decreases the transmission of light. Various national security related applications encounter adverse fog conditions. Fog causes a significant security concern for any national security locations that are located near or in coastal waters. Circular polarization techniques can provide additional detection range in these environments, as is demonstrated in this report. Naval systems can benefit from the use of circular polarization systems when fog conditions decrease visibility. In heavy fog conditions visibility may decrease to mere feet. This is a major security concern for any individuals, boats, or buildings where visible security systems become useless. Coupling circular polarization imaging systems to traditional imaging systems can increase detection range in these environments and detect approaching unfriendly objects at a larger and safer distance. Circular polarization can also be utilized in LIDAR systems to increase range in heavy fog conditions. Circular polarization persists longer than linear polarization in both radiation and advection fog. Future LIDAR systems can utilize these results to better design systems for use in fog environments. The performance of circular polarization is wavelength dependent and several technically relevant wavelengths can be exploited for enhancing signal persistence and imaging distances. Designing a LIDAR system for fog conditions can utilize the results in this report to best determine the laser wavelength and detector for maximum benefit from circular polarization. The use of circular polarization is very promising in fog environments.

Similar to fog environments, imaging in dust environments are also very challenging. Dust is a major issue in desert environments. Dust storms can cause extreme decreases in visibility much like heavy fog. Dust is also a major issue in brownout conditions occurring when aircraft attempt to take off or land in desert environments. Tailoring imaging systems to utilize circular polarization in dust conditions can increase the detection range and contrast utilizing circular polarization techniques. As with fog conditions, for any national security locations where dust storms or high dust conditions are present increasing detection range is valuable. Circular polarization LIDAR systems can be utilized to increase the ranging capability while landing the aircraft. Circular polarization can be beneficial in multiple scattering environments.

The anticipated impact of this work will support DS&A/IDAPR Airborne Intelligence, Surveillance, and Reconnaissance for tactical situational awareness in challenging environments for improved target identification. This work offers insight into solutions for imaging in traditionally difficult environments such as coastal settings with water interfaces and fog. Future work will also explore extending this technique to other turbid or scattering environments, such as dust and smoke.

This work will ultimately enable imaging systems with improved target identification and discrimination for Airborne Intelligence, Surveillance, and Reconnaissance (ISR) to work through traditionally difficult environments and have broad impact over a range of DOE and intelligence airborne and satellite programs (e.g., SOCOM, Air Force, NRO, NASA). For example, US Special Operations Forces have identified challenges – which can be addressed within 5 years – that include LIDAR in all environments, day/night.

CONCLUSION:

Through the use of polarization tracking Monte Carlo simulations we have shown that there are clear wavebands where circular polarization persists in the intended polarization state superiorly compared to linear polarization for highly scattering environments representative of fog and dust. All four environments of interest show possible wavelength bands where circular polarization can be utilized to increase detection range. Radiation fog has wavebands available in the entire IR spectrum. All three particle sizes simulated (1, 4, and 10 microns) show a preference for circular polarization in the SWIR, while only the 4 and 10 micron particles show a preference in the MWIR, and only the 10 micron particle exhibits superior persistence for circular polarization in the LWIR. All three particle sizes in the advection fog model (10, 20, and 40 microns) show a preference for circular polarization at SWIR wavelengths and LWIR wavelengths of 7 to 11 microns. The persistence of circular polarization is not as positive for the two dust models. Only the 6 micron particle size results from the small particle Sahara dust shows persistence benefits in the MWIR, 7 to 9 microns, and 10.5 to 12 micron wavelengths. Lastly, for the large particle sizes of Sahara dust (10, 20, and 30 microns) at a wavelength of roughly 4 microns all three particle sizes show superior persistence for circular polarization.

This work breaks from previously published works and offers new insight into potential environments and wavebands of interest where circular polarization can be utilized to increase detection range. Previous research has focused on limited wavelengths in the visible region with underwater scattering environments typically utilizing polystyrene microspheres, milk, or tissue phantoms as scattering objects. We have produced simulation results supporting broad wavelength responses for particle sizes and refractive indices representative of natural scattering environments where circular polarization persists longer than linear polarization.

This work looks to inspire continued interest in circular polarizations benefits in various applications involved in scattering environments, specifically increasing detection range. Future work includes further simulation work with polydisperse distributions of scattering particles, and experimental work in real world scattering environments utilizing circular polarization.

References

1. G. D. Gilbert and J. C. Pernicka, "Improvement Of Underwater Visibility By Reduction Of Backscatter With A Circular Polarization Technique," in

Underwater Photo Optics I (International Society for Optics and Photonics, 1966), pp. 15–25.

2. G. D. Gilbert and J. C. Pernicka, "Improvement of underwater visibility by reduction of backscatter with a circular polarization technique.," Appl. Opt. **6**, 741–6 (1967).

3. S. Q. Duntley, "Underwater visibility and photography," in *Optical Aspects of Oceanography* (Academic Press, 1974), pp. 138–149.

4. J. S. Tyo, "Enhancement of the point-spread function for imaging in scattering media by use of polarization-difference imaging.," J. Opt. Soc. Am. A. Opt. Image Sci. Vis. **17**, 1–10 (2000).

5. M. P. Silverman and W. Strange, "Object delineation within turbid media by backscattering of phase-modulated light," Opt. Commun. **144**, 7–11 (1997).

6. M. Dubreuil, P. Delrot, I. Leonard, A. Alfalou, C. Brosseau, and A. Dogariu, "Exploring underwater target detection by imaging polarimetry and correlation techniques.," Appl. Opt. **52**, 997–1005 (2013).

7. V. Sankaran, K. Schönenberger, J. T. Walsh, and D. J. Maitland, "Polarization discrimination of coherently propagating light in turbid media.," Appl. Opt. **38**, 4252–61 (1999).

8. V. Sankaran, J. T. Walsh, and D. J. Maitland, "Comparative study of polarized light propagation in biologic tissues.," J. Biomed. Opt. **7**, 300–6 (2002).

9. S. Bartel and A. H. Hielscher, "Monte Carlo simulations of the diffuse backscattering mueller matrix for highly scattering media.," Appl. Opt. **39**, 1580–8 (2000).

10. G. D. Lewis, D. L. Jordan, and P. J. Roberts, "Backscattering target detection in a turbid medium by polarization discrimination.," Appl. Opt. **38**, 3937–44 (1999).

11. S. Kartazayeva, X. Ni, and R. Alfano, "Backscattering target detection in a turbid medium by use of circularly and linearly polarized light.," Opt. Lett. **30**, 1168–70 (2005).

12. D. Bicout, C. Brosseau, A. Martinez, and J. Schmitt, "Depolarization of multiply scattered waves by spherical diffusers: Influence of the size parameter," Phys. Rev. E **49**, 1767–1770 (1994).

13. A. Ishimaru, S. Jaruwatanadilok, and Y. Kuga, "Polarized pulse waves in random discrete scatterers.," Appl. Opt. **40**, 5495–502 (2001).

14. D. Miller and E. L. Dereniak, "Selective polarization imager for contrast enhancements in remote scattering media.," Appl. Opt. **51**, 4092–102 (2012).

15. J. Fade, S. Panigrahi, A. Carré, L. Frein, C. Hamel, F. Bretenaker, H. Ramachandran, and M. Alouini, "Long-range polarimetric imaging through fog.," Appl. Opt. **53**, 3854–65 (2014).

16. J. S. Tyo, D. L. Goldstein, D. B. Chenault, and J. A. Shaw, "Review of passive imaging polarimetry for remote sensing applications.," Appl. Opt. **45**, 5453–69 (2006).

17. M. Xu and R. Alfano, "Circular polarization memory of light," Phys. Rev. E **72**, 065601 (2005).

18. J. D. van der Laan, D. A. Scrymgeour, S. A. Kemme, and E. L. Dereniak, "Range and contrast imaging improvements using circularly polarized light in scattering environments," in *SPIE Defense, Security, and Sensing*, G. C. Holst and K. A. Krapels, eds. (International Society for Optics and Photonics, 2013), p. 87060R.

19. C. Bohren and D. Huffman, *Absorption and Scattering of Light by Small Particles* (John Wiley & Sons, Inc., 1983).

20. K. Beier and H. Gemperlein, "Simulation of infrared detection range at fog conditions for Enhanced Vision Systems in civil aviation," Aerosp. Sci. Technol. **8**, 63–71 (2004).

21. R. A. Chipman, "Polarimetry," in *Handbook of Optics* (1995), p. Vol. 2, Chap. 22.

22. J. C. Ramella-Roman, S. A. Prahl, and S. L. Jacques, "Three Monte Carlo programs of polarized light transport into scattering media: part I.," Opt. Express **13**, 10392–405 (2005).

23. M. Al Naboulsi, H. Sizun, and F. de Fornel, "Fog attenuation prediction for optical and infrared waves," Opt. Eng. **43**, 319 (2004).

24. D. Deirmendjian, "Scattering and polarization properties of water clouds and hazes in the visible and infrared," Appl. Opt. **3**, 187 (1964).

25. D. L. Hutt, "Estimation of aerosol microphysical parameters from visible and infrared extinction measurements," in *SPIE's 1996 International Symposium on Optical Science, Engineering, and Instrumentation*, C. Dainty and L. R. Bissonnette, eds. (International Society for Optics and Photonics, 1996), pp. 503–514.

26. D. Segelstein, "The complex refractive index of water," University of Missouri (1981).

27. B. Weinzierl, A. Petzold, M. Esselborn, M. Wirth, K. Rasp, K. Kandler, L. Schütz, P. Koepke, and M. Fiebig, "Airborne measurements of dust layer properties, particle size distribution and mixing state of Saharan dust during SAMUM 2006," Tellus B **61**, 96–117 (2009).

28. A. Ivanov, "Polarization of light and its use in various problems of optics of scattering media," Opt. Spectrosc. **107**, 171–183 (2009).

29. F. E. Volz, "Infrared optical constants of ammonium sulfate, sahara dust, volcanic pumice, and flyash.," Appl. Opt. **12**, 564–8 (1973).

Sandia National Laboratories is a multi-program laboratory managed and operated by Sandia Corporation, a wholly owned subsidiary of Lockheed Martin Corporation, for the U.S. Department of Energy's National Nuclear Security Administration under Contract DE-AC04-94AL8500.